11-2017

Tetragonal Diiodotetrapyridinedicopper(I): Structure, Luminescence, and Computational Modeling

Andrew W. Kelly

Joseph V. Handy

Aaron D. Nicholas

et al.

Robert D. Pike

HARVEY SPECIAL ISSUE

Tetragonal Diiodotetrapyridinedicopper(I): Structure, Luminescence, and Computational Modeling

Andrew W. Kelly,[a] Joseph V. Handy,[a] Aaron D. Nicholas,[b] Francis H. Barnes,[b] Howard H. Patterson,[b] Lukasz Wojtas,[c] and Robert D. Pike,[a]*

[a]*Department of Chemistry, College of William and Mary, Williamsburg, VA 23187-8795.* [b]*Department of Chemistry, University of Maine, Orono, ME 04469-5706.* [c]*Department of Chemistry, University of South Florida, Tampa, FL 33620.*

Corresponding Author: Robert D. Pike

Department of Chemistry

College of William and Mary

Williamsburg, VA 23187-8795.

telephone: 757-221-2555

FAX: 757-221-2715

email: rdpike@ wm.edu

Keywords: copper(I) iodide; pyridine; dimer; polymorph; luminescence; X-ray crystal structure; density functional theory

Abstract:

We report on a new crystal modification of $(CuIPy_2)_n$ (Py = pyridine), a compound first reported by White *et al*. In contrast to White's orthorhombic structure, which is comprised of rhomboid iodide-bridged dimers, $Cu_2I_2Py_4$, our new tetragonal crystal structure in space group $P4_12_12$ is disordered and can be interpreted as either iodide-bridged dimers or helical chains. To determine the structure type, variable temperature X-ray diffraction and luminescence measurements were carried out. The photoluminescence spectrum shows a distinct cluster-centered transition at high excitation energies which is consistent with the dimer structure. DFT and TD-DFT calculations were performed to explain the difference between the emission spectrum at high energies compared to low energies. Furthermore, correlation of the luminescence spectrum with the X-ray results as temperature is varied demonstrates that the cluster-centered luminescence band in $Cu_2I_2Py_4$ arises from close Cu···Cu distances which vary with temperature. A low temperature X-ray crystallographic redetermination of the cubane tetrameric $Cu_4I_4Py_4$ is also presented. Both $Cu_2I_2Py_4$ and $Cu_4I_4Py_4$ structures show distortion of the Cu_nI_n core cluster at low temperature resulting in reduced Cu···Cu distances, but with I···I distances roughly unchanged.

Introduction:

The copper(I) halide complexes of substituted pyridine ligands have been well studied both because of their rich structural diversity, and the fact many of these complexes exhibit intense photoluminescence. Thus, the cubane tetramer $Cu_4I_4Py_4$ (Py = pyridine, type I in Chart 1) shows six close Cu···Cu distances ranging between 2.619 and 2.721 Å [1], all of which are within the 2.8 Å van der Waals radius sum for copper [2]. This complex shows interesting photoluminescence behavior. At 77 K, its spectrum is dominated by a high energy emission band located in the blue region. Computational work has shown that this band is associated with halide to ligand (Py) charge transfer (XLCT) behavior [3]. The band is not observed when an aliphatic amine, such as piperidine, is coordinated in place of Py. The high energy XLCT band observed in $Cu_4I_4Py_4$ is highly thermochromic, and its greatly reduced intensity at ambient temperature reveals a dominant low energy yellow emission. The non-thermochromic low energy emission band results from a combination of halide to metal charge transfer (XMCT) and intra-metal (d → s,p) character. Since it is associated with the core Cu_nI_n cluster (n = 4), the band is referred to as cluster centered (CC). A second 1:1 CuI:Py complex is known and takes the form of an infinite stair step polymer, type II in Chart 1 [4]. Interestingly, its previously reported emission spectrum shows a single broad feature at 450 nm [4]. This non-thermochromic band is assigned to a mixed halide/metal-to-ligand charge transfer (XMLCT) transition. CC transitions appear to be absent in this case.

Chart 1. Structures of CuI-Py Complexes

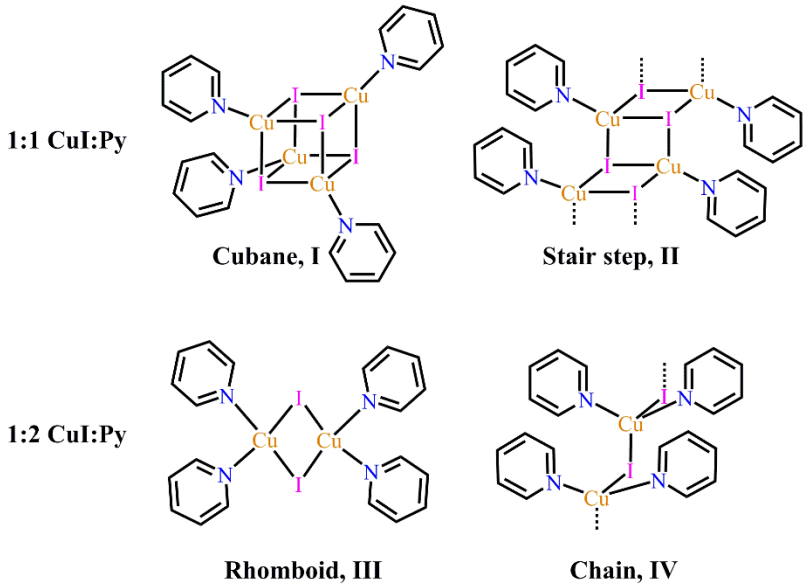

The 1:2 CuI:Py complex, **1b**, was first reported by White *et al.* in 1984 as an iodide-bridged dimer, $Cu_2I_2Py_4$, rhomboid form, type III in Scheme 1 [5]. Compound **1b** was prepared by concentration of a solution of CuI in Py. Subsequently, Ford *et al.* replicated the synthesis, precipitating the product as a powder through the addition of hexane to the CuI/Py solution [3]. They further reported its emission spectrum as consisting of a broad non-thermochromic LE band centered at 502 nm, consistent with CC behavior. There was no evidence of an XLCT band. The **1b** dimer structure has not been re-determined since White's work. Importantly, White claimed that "[c]rystals were badly twinned and attempts to obtain a monocrystalline specimen unsuccessful; eventually, data were measured by deconvolution of the diffraction pattern at high 2θ of a twinned specimen and the structure solved, showing the complex to be a dimer." [5]

As part of our studies on the highly emissive complexes of CuI, we have prepared crystals of the 1:2 complex of CuI:Py and determined their structure and photophysical behavior. Here we report a new polymorph of 1:2 CuI:Py, **1a**, distinct from White's polymorph, **1b**. It can be interpreted from the X-ray crystal structure as either a rhomboid dimer (type III) or as a Py-decorated, single-stranded iodide-bridged

chain (type IV, see Chart 1). In order to determine the correct interpretation, we report temperature dependent structure determinations in conjunction with variable temperature photoluminescence results for **1a**, as well as computational results. Additionally, we report the first low temperature X-ray structure determination of $Cu_4I_4Py_4$, **2**, and discuss behavior of the Cu_nI_n clusters with changing temperature.

Experimental:

General:

All reagents were purchased from Aldrich or Acros and were used as received. Pyridine was distilled before use. Atomic absorption copper analysis was carried out as previously described [6]. Thermogravimetric analyses (TGA) were conducted using a TA Instruments Q500 in the dynamic (variable temp.) mode with a maximum heating rate of 50 °C/min. to 500 °C under 60 mL/min. N_2 flow. Steady-state photoluminescence spectra were recorded with a Model QuantaMaster-1046 photoluminescence spectrophotometer from Photon Technology International. The instrument is equipped with two excitation monochromators and a single emission monochromator with a 75 W xenon arc lamp. Low temperature steady-state photoluminescence measurements were achieved by using a Janis St-100 optical cryostat equipped with a Honeywell temperature controller. Liquid nitrogen was used as coolant.

Synthesis and Crystallization.

*$[Cu_2I_2Py_4]$, **1a**:* CuI (190 mg, 1.00 mmol) was dissolved in 1.5 mL Py. The yellow solution was filtered and layered with ethyl ether and allowed to crystallize. After one day, colorless block crystals had formed. Alternatively, a bulk powder was formed via careful dropwise addition of ether to the CuI/Py solution until powder started to form, and then continuing slow addition until no more solid appeared. The solids were handled only briefly in air, as they readily lost Py to form $Cu_4I_4Py_4$ (**2**). Yield = 303 mg (0.435 mmol, 86.9%). %Cu (AAS) 19.4 (calcd 18.1). TGA Calcd for ½ $Cu_4I_4Py_4$: 77.1. Found: 77.1 (40–90 °C). Calcd for CuI: 54.5. Found: 54.8 (90–150 °C).

*$[Cu_4I_4Py_4]$, **2**:* CuI (190 mg, 1.00 mmol) was dissolved in 1.5 mL Py. The yellow solution was filtered and an excess of ethyl ether was added, immediately precipitating a white powder which was collected and washed with additional ether and dried under vacuum. (156 mg, 0.145 mmol, 57.8%). %Cu (AAS) 24.0 (calcd 23.4). TGA Calcd for CuI: 70.7. Found: 70.9 (90–140 °C). X-ray quality crystals were grown by diffusion of ethyl ether into an acetone solution of the complex.

X-ray Crystallography.

Crystals were mounted on glass fibers and quickly transferred to the diffractometer with sample cold stream running. All measurements were made using graphite-monochromated Mo Kα radiation on a Bruker-AXS three-circle Apex DUO diffractometer, equipped with a SMART Apex II CCD detector. Initial space group determination was based on a matrix consisting of 36 frames. The data were reduced using SAINT+ [7], and empirical absorption correction applied using SADABS [8].

Structures were solved using intrinsic phasing. Least-squares refinement for all structures was carried out on F^2. The non-hydrogen atoms were refined anisotropically. Hydrogen atoms were located in the Fourier difference map and then allowed to refine isotropically. Structure solution was carried out using SHELXTL [9] and refinement was performed using the ShelXle program [10]. Details of the X-ray experiments and crystal data are summarized in Tables 1 and S1. Selected bond lengths and bond angles are given in Tables 2 and 3. Crystallographic data for the structures reported herein have been deposited with the Cambridge Crystallographic Data Centre and allocated the deposition numbers CCDC 1529200-1529204. These data can be obtained free of charge from the Cambridge Crystallographic Data Centre via www.ccdc.cam.ac.uk/data_request/cif.

Powder diffraction was carried out on the instrument described above using a Cu Imμs source. Samples were ground and prepared as mulls using Paratone N oil. Three 180 s frames were collected,

covering 8–70° 2θ. Frames were merged using the Apex III software and were further processed using Diffrac-EVA software [11]. Simulated powder patterns from single crystal determinations were generated using Mercury [12].

DFT Calculations.

Density Functional Theory (DFT) calculations were performed for a $Cu_2I_2Py_4$ dimer along with a single cubane $Cu_4I_4Py_4$ using Gaussian 09 at the University of Maine supercomputing group. X-ray structural data were used as initial input. Ground state and excited state geometries were obtained using the LANL2DZ basis set with the hybrid density functional theory due to Becke's 3-parameter nonlocal exchange functional with the non-local correlation functional of Lee, Yang and Parr, B3LYP, for all atoms [13]–[15]. Molecular orbitals were also calculated using Gaussian 09. Optimized ground state structures were used for vertical energy calculations using the time dependent DFT (TD-DFT) method. Avogadro software (version 1.1.1) was used for molecular orbital visualization. Optimized ground state geometries were compared to X-ray structural data to validate our models. In addition, we have calculated the infrared spectrum and absorption spectra.

Diffuse Reflectance Spectroscopy

Diffuse reflectance UV-visible spectra were collected on solid samples at 298 K. The light source was a Mikropack DH-2000 deuterium and halogen light source coupled with an Ocean Optics USB4000 detector. Collected light was collected with a fiber optic cable. Spectra was referenced with PTFE. Data was processed using SpectraSuite 1.4.2_09.

Infrared Spectroscopy

Infrared spectra were collected on solid samples at 298 K using a Perkin Elmer FT-IR Spectrum Two equipped with a Universal Attenuated Total Reflectance (UATR) accessory consisting of a ZnSe crystal with a 2 micron path length. The detector is a $LiTaO_3$ MIR detector. Spectra were collected between 450 cm^{-1} and 4,000 cm^{-1} at a 2 cm^{-1} resolution.

Results and Discussion:

Syntheses and Structures.

Copper(I) iodide readily dissolves in pyridine (Py) to form a yellow solution. From this solution either the ligand-rich phase $CuIPy_2$ (**1**) or the metal-rich phase $Cu_4I_4Py_4$ (**2**) can be precipitated through the addition of ethyl ether, depending on the experimental conditions. Rapid addition of ether produces **2** as a white solid having intense yellow luminescence under 365 nm irradiation. In contrast, slow diffusion of ether into the CuI/Py solution produces colorless block crystals identified as polymorph **1a**. Under 365 nm irradiation, the crystals show a moderately intense green luminescence emission. As has been reported [3], this 1:2 CuI:Py complex undergoes loss of Py over the course of several hours when left in open air, according to reaction (1). The product after Py loss is the 1:1 compound $Cu_4I_4Py_4$, **2**.

$$4\ CuIPy_2\ (s) \rightarrow Cu_4I_4Py_4\ (s) + 4\ Py\ (g) \qquad (1)$$

The surprising aspect of $CuIPy_2$, as prepared in this way, is that the tetragonal X-ray crystal structure of **1a** does not match White's reported orthorhombic crystal structure, **1b** [5], see Table 1. Comparison of the theoretical powder patterns generated from the two structures showed no overlap (see Figure S1). Thus, the structures are polymorphs. Also surprisingly, we were unable to produce White's originally reported **1b** crystals. Multiple attempts at crystallization using solutions of CuI/Py according to White's published method yielded only the tetragonal polymorph. To determine whether **1a** was the major polymorph under the preparative conditions used, powder diffraction was carried out on a freshly crystallized sample. As

shown in Figure 1, a very good match was seen between the experimental data and the calculated powder pattern for **1a**. Although traces of polymorph **1b** cannot be ruled out (see overlay Figure S2), it is clear that the vast majority of the sample consists of polymorph **1a**.

Figure 1. X-ray powder diffraction overlay: Freshly precipitated $CuIPy_2$ (upper trace in red) and calculated powder pattern for **1a** (lower trace in black).

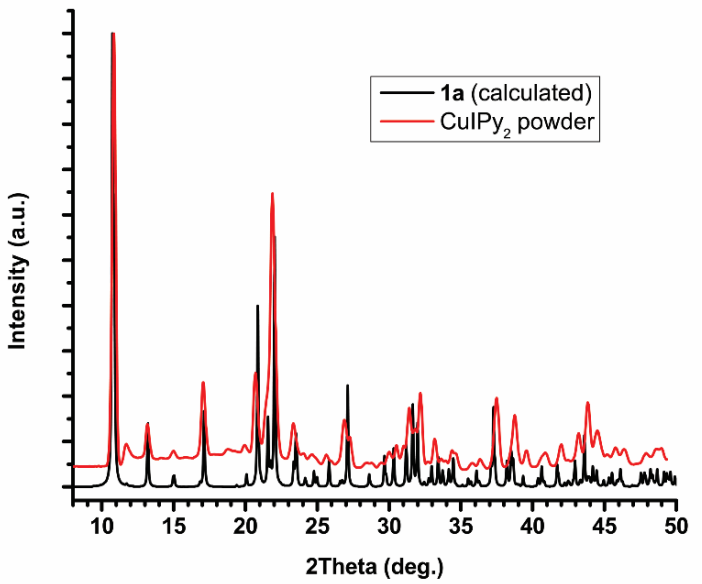

Crystals of the new polymorph, **1a**, like those of **1b**, showed a strong tendency toward twinning. In fact, twinning was apt to produce falsely-reduced symmetry. Solution of a twinned **1a** crystal in tetragonal space group $P4_1$ yielded a fairly good quality structure, showing $Cu_2I_2Py_4$ dimers. However, a rather high wR2 value of near 13% and the presence of four independent dimer molecules, suggested that this might not, in fact, be the true structure solution. Careful cutting of block crystals into thin plates yielded data that solved in tetragonal space group $P4_12_12$. In this higher symmetry cell, the *a*- and *b*-axes are shortened by half and only a single crystallographically independent dimer unit is present. Additionally, the final wR2 refined to near 3%. Nevertheless, even this cut crystal still showed moderate racemic twinning.

The structure of **1a** showed very interesting positional disorder affecting all atoms. Disordered $CuPy_2$ fragments are related by 2_1 screw symmetry. Bi-positional disorder allows the resulting atom map to be interpreted according to two equally valid models: that of iodide-bridged dimers, $Cu_2I_2Py_4$, or iodide-bridged chains $(CuIPy_2)_n$. The situation is illustrated in Figure 2, where it can be seen that replacing dimers with chains is a matter of which set of disordered $CuPy_2$ fragments is chosen. Of note is the fact that in the dimer solution, close Cu···Cu interactions are evident, see Tables 2 and 3. No such interactions are seen in the chain solution, either within or between chains.

Figure 2. X-ray structure of **1a** viewed along the *a*-axis. Disorder allows for interpretation as iodide-bridged dimer units (top) or chains (bottom). Ball and stick *vs.* wireframe is used to emphasize the disorder. Carbon and hydrogen atoms omitted for clarity. Color scheme: copper = orange, iodine = purple, nitrogen = blue.

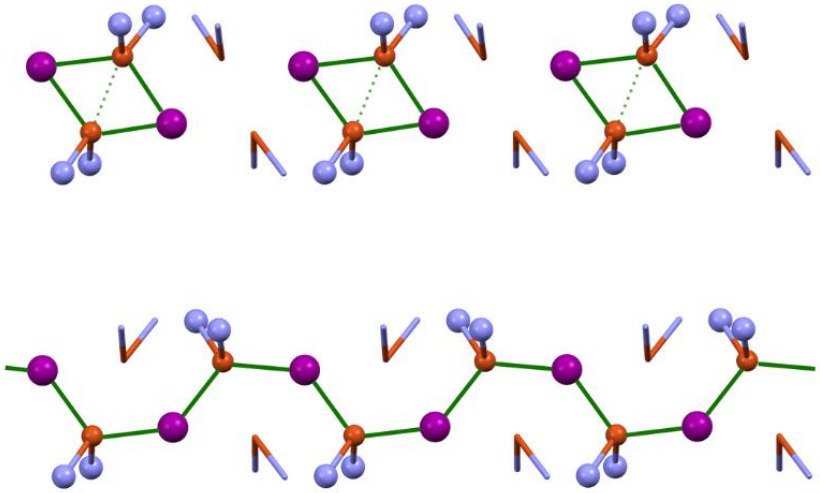

For **1a** the assignment of dimer versus chain structure for $CuIPy_2$ cannot be made on the basis of crystallographic data alone. Unfortunately, the high ligand lability of the Cu(I) complexes, as exhibited by the facile loss of Py from **1a**, precluded the use of mass spectrometry in determining oligomer size. The choice of dimers (type III in Chart 1) as the more likely bonding arrangement is supported by the prevalence of $Cu_2I_2(XPy)_4$ dimers in the literature for substituted pyridines (XPy) and the near absence of

$[CuI(XPy)_2]_n$ chains (type IV). A search of the Cambridge Crystallographic Database [16] for pyridine-substituted CuI revealed roughly 50 rhomboid dimer-based structures [5],[17]. In contrast, only a single chain structure, $[(CuI)_2$(tetra-4-(4-pyridyl)phenylmethane)], has been identified [18]. Moreover, in the latter case the chain structure was found to be a kinetic product, spontaneously and irreversibly rearranging to the more densely-packed dimer form. However, to confirm **1a** as a dimeric structure additional characterization was required.

Diffuse Reflectance Spectroscopy Studies

We collected the diffuse reflectance spectrum (DRS) of **1a** and in Figures 3 and S7 show the Fresnel transformed absorbance spectrum. The presence or absence of a CC transition should enable differentiation between the dimer or chain configurations. This is because CC bands are unique to cluster configurations and thus would strongly support a dimer assignment. Absorption spectra reveal a very broad and highly intense peak with a maximum at 335 nm, a lower intensity narrow shoulder at 262 nm, and another peak at 425 nm. Deconvolution of this spectrum allows for easier interpretation and assignment of these transitions. The broad peak at 335 nm is most likely a XMLCT transition, and would be observed for either the chain or the dimer configuration. The more interesting feature of the DRS absorption spectrum is the partially obscured shoulder at 262 nm. This low intensity and narrow peak is most reminiscent of a CC transition, which occurs at higher energies than those associated with MLCT transitions and has been previously reported for cubane **2** [25]. Therefore, the absorbance spectrum offers the first piece of evidence of the type III dimer configuration. The remaining peak at 425 nm can thus be assigned to as a XLCT.

Figure 3: Diffuse reflectance spectrum of **1a** at 298 K (solid line). Experimental data (solid line) is shown with deconvoluted bands (dashed line).

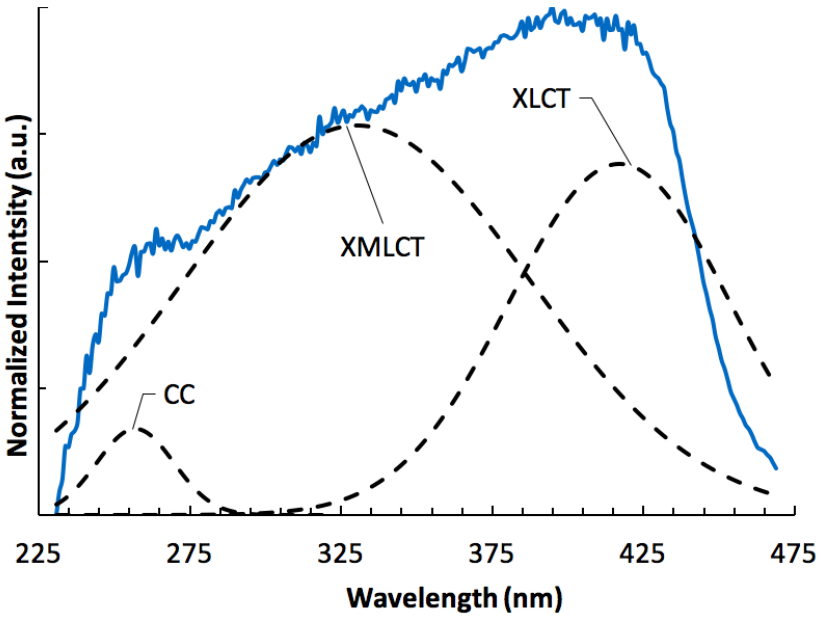

Luminescence Studies.

Because of the ambiguity in the X-ray structural data, luminescence measurements were used to determine whether **1a** exists as a dimer (type III) or chain (type IV) configuration. We would expect to observe drastically different luminescence spectra and temperature dependence for these structures. Chain configurations would be expected to show a single XMLCT emission and excitation combination that does not undergo a shift in emission energy with temperature. In contrast, dimer configurations luminesce similarly to the well-known tetramer complex **2** due to the presence of individual metal-halide clusters (Figure S5), their spectra consisting of a high energy emission band and a low energy emission band at 78 K [3]. White and Ford have assigned these emission bands to a XLCT and a mixed XMCT cluster-centered

(CC) transition, respectively. In these studies upon heating **2** to ambient temperature the high energy XLCT band is lost, while a blue shift of the low energy CC band occurred.

Luminescence measurements for **1a** (Figure 4 and 5) performed at 394 nm excitation and 78 K show a single broad emission peak at 500 nm. This prominent peak is reduced in intensity as the temperature is increased, but no wavelength shift is observed. Due to the lack of emission energy shift, we assign this transition as a XMLCT band [19]. Upon changing the excitation wavelength to 340 nm, distinctly different emission peaks are observed. The emission band at 500 nm remains unaltered; however, at 78 K two additional peaks at 435 nm and 607 nm are observed. The high energy band at 435 nm is observed only at temperatures below 103 K. The low energy band is present throughout the studied temperature range and undergoes a blue shift of 22 nm, from 607 nm to 583 nm, upon warming the sample from 78 K to 173 K. The energies and temperature dependence of these emission peaks are very similar to those reported for the well-known tetrameric complex **2** [3]. Accordingly, we assign the high energy peak at 435 nm to a XLCT transition, while the low energy peak at 607 nm is assigned to a CC transition [3]. The presence of a CC band, which is only possible in a Cu_nI_n cluster, confirms that **1a** is configured as a dimer.

Figure 4: Luminescence spectra of **1a** between 78 K and 298 K. Emission spectra (solid lines) were obtained with excitation at 394 nm and excitation spectra (dashed lines) were obtained with emission at 500 nm.

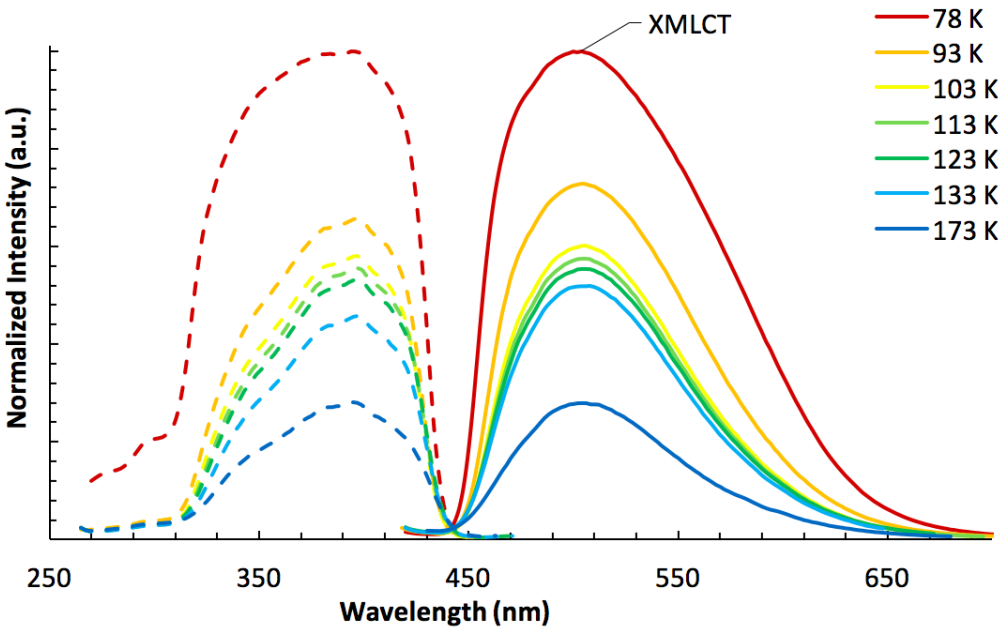

Figure 5: Luminescence spectra of **1a** between 78 K and 298 K. Emission spectra (solid lines) were obtained with excitation at 340 nm and excitation spectra (dashed lines) were obtained with emission at 434 nm.

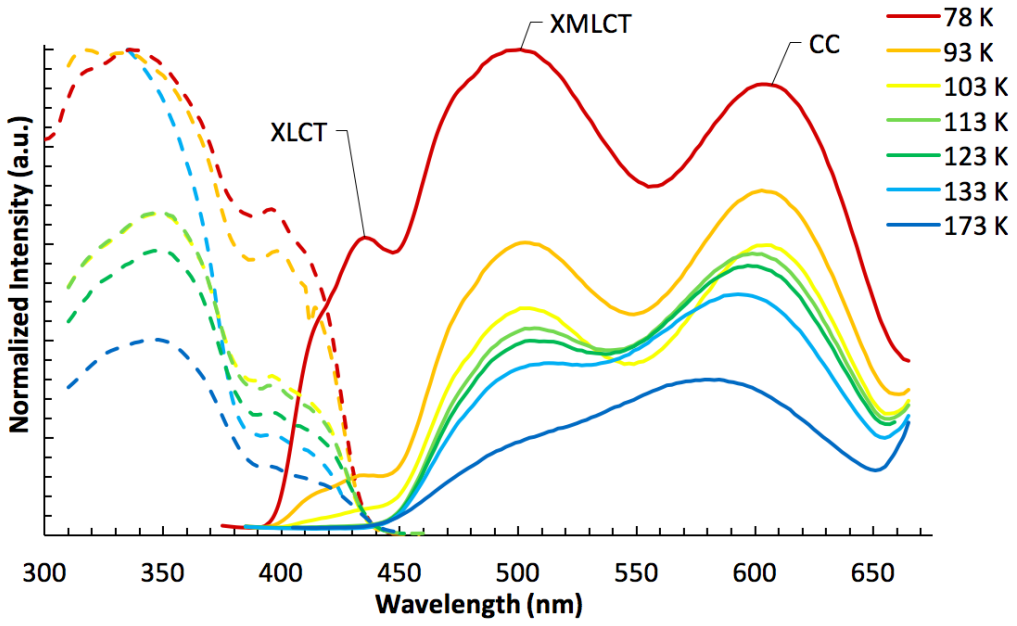

Computational Studies.

We have performed DFT and TD-DFT calculations on a dimer model of **1a** to explore the assignments of the emission bands observed in the luminescence spectra. Our model is in good agreement with experimental data. Ground state geometry computational results for **1a** (Figure 6), which are summarized in Table 4, show a partially distorted tetrahedral copper(I) center coordinated to two nitrogen atoms and two iodine atoms. The slight distortion of the tetrahedron is apparent in the reduced N–Cu–I angle of ~107°. Dimeric Cu_2I_2 clusters form planar rhombic metal-halide centers with μ_2-bridging I atoms [17]. Calculated atom···atom distances for the rhombic centers are in agreement to the experimental values. The calculated Cu···Cu distance of 2.88 Å for the **1a** dimer is in good agreement with the experimental value, which ranges from 2.67 to 2.71 Å between 100 and 250 K (see Table 3 below). The structural accuracy of our dimer model is further supported by the agreement between the TFD-calculated and experimental infrared spectra (Figure S6).

Figure 6: Ground state geometries of the **1a** dimer viewed along (**A**) the X-axis and (**B**) ⊥ to the $[Cu_2I_2]$ plane. Hydrogen atoms removed for clarity, see Figure 1 for color scheme.

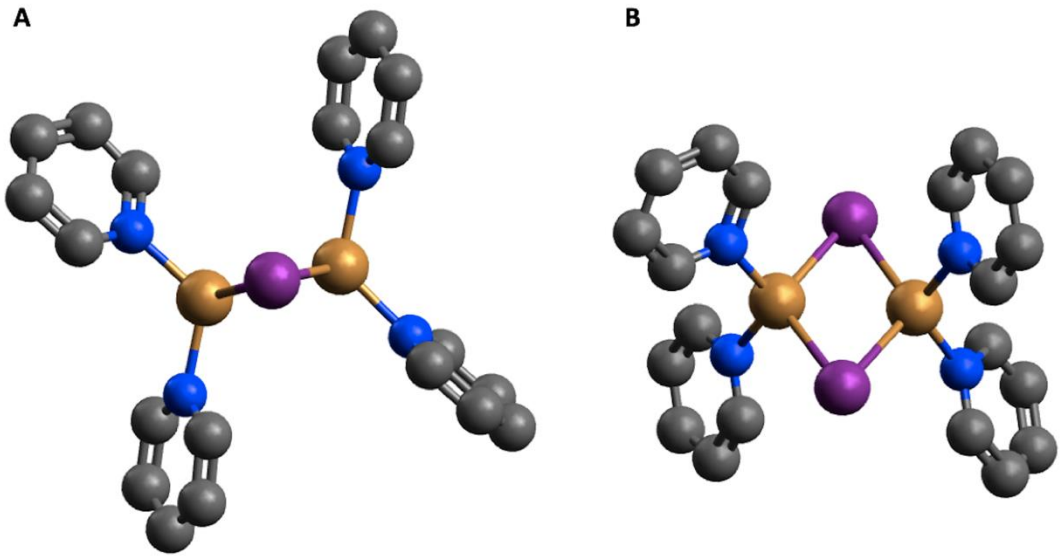

The TD-DFT-calculated absorption spectrum of **1a** is shown in Figure S7. Absorption calculations for the dimer are in good agreement with the experimental data. In this spectrum we observe a calculated broad high-intensity peak at 400 nm with a less prominent peak at 267 nm. Deconvolution of this spectrum results in three peaks at 264, 343, and 408 nm which are similar in energy to the deconvoluted experimental data. Molecular orbital calculations at each of these absorption energies were performed (Figure S8-10 and Table S2-3). Only excited states at corresponding absorption energies with an f-oscillation value >0.01 are considered for MO calculations. These calculated states are at 400, 338, and 267 nm. For each of these energies, we calculated distinctly different MO transitions. At 400 nm we clearly see a predominant XLCT type transition with negligible MLCT contributions. These XLCT transition types account for 82.4% of the total contribution and confirm our XLCT assignment of this absorption peak. Upon increasing the energy to 338 nm, the MO contribution shifts to a dominant MLCT (71.0%) with the remaining contribution being both a XMLCT and XLCT transition (29.0%). This 71.0%/29.0% split strongly supports our mixed XMLCT assignment of this peak. Finally, calculated MOs at 269 nm reveal a complex metal-halide MO rearrangement for all transitions. Specifically, MO calculation results predict that, upon excitation, electrons from the Cu 3d/I 5p atomic orbitals populate the Cu 4s/3p AOs. Rearrangement of the Cu_2I_2 cluster is defined as a CC transition and strongly supports this assignment of the band at 268 nm. In summary, we assign the absorption peaks at 400, 338, and 267 nm to XLCT, XMLCT, and CC transitions, respectively. Our peak assignments for **1a** agree with the previously-reported DFT and TD-DFT calculations for the cubane **2** [25]. The various XLCT, XMLCT, or CC absorption bands help explain the difference in emission spectra between 394 nm and 340 nm and show that emission energy is tunable by adjusting the excitation energy.

Figure 7: Representative calculated MO transition at 400 nm (top), 338 nm (middle), and 269 nm (bottom). Full MO calculation results can be found in Figure S9.

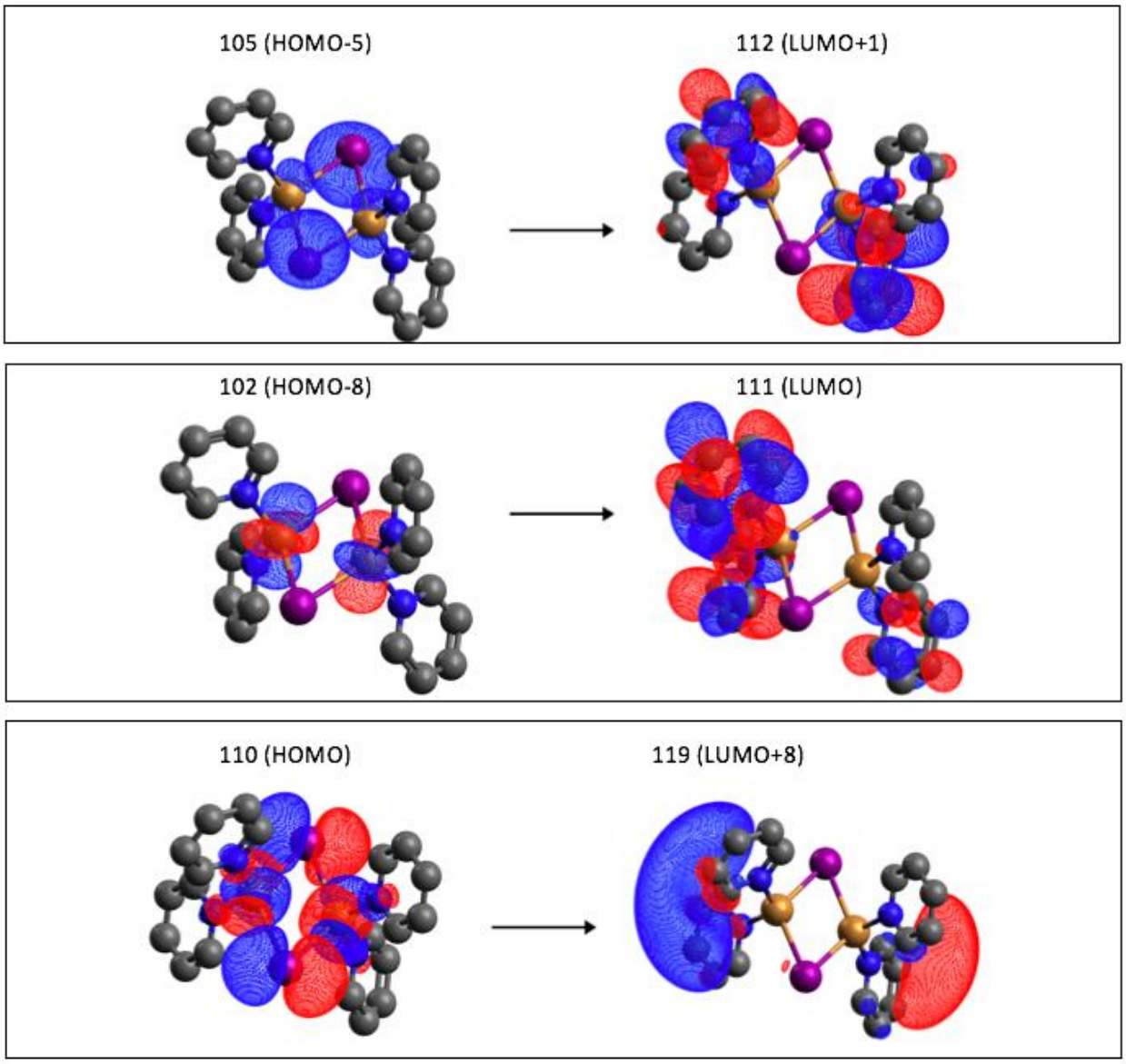

Temperature Dependent Studies

In order to better understand the atomic interactions within the central cluster in **1a**, its X-ray structure was determined at 100, 150, 200, and 250 K, see Table S1. The dimeric structure of **1a**, determined at 100 K, is shown in Figure 8. Selected bond lengths and angles for the **1a** dimer structure determined at the four temperatures are given in Table 3. Comparison of these data to one another and to those of **1b** at ambient temperature is instructive. Bond lengths are typically expected to lengthen as

temperature is increased. This is generally the case for **1a**. However, some interesting behavior is seen that can be attributed to flexing of the Cu_2I_2 cluster core as the temperature changes. The Cu···Cu distance steadily lengthens with increasing temperature, increasing from 2.6686(9) Å at 100 K to 2.7129(12) Å at 250 K, while remaining within the van der Waals radius sum. However, I···I separation shows no change within experimental precision between 100 (4.525(5) Å) and 150 K (4.530(5) Å), but above this temperature is seen to shorten greatly, decreasing to 4.479(5) Å at 250 K. This trend is presumably shaped by two competing effects. The tendency of the I···I distance to lengthen with increasing temperature is ultimately overcome by reshaping of the rhomboid ring as the Cu atoms move apart, see Figure 9. Accordingly, the Cu–I–Cu angle is seen to increase with temperature, while the I–Cu–I angle contracts. Comparing bond length data of polymorphs **1a** and **1b**, we see that the ambient temperature Cu···Cu in **1b** is nearly identical to that of **1a** at 100 K. Consistent with the ring flexing associated with a short Cu···Cu distance in **1b**, its I···I is longer than that of **1a** seen at any temperature.

Figure 8. Thermal ellipsoid (50%) drawing of **1a** at 100 K treated as a dimer.

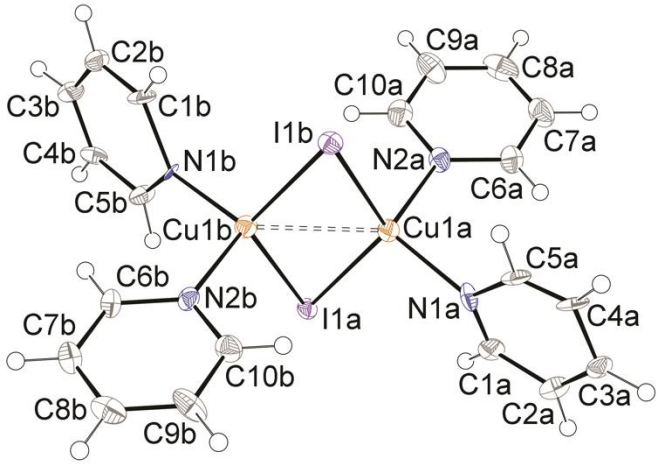

Figure 9. Flexing behavior of the Cu_2I_2 core in **1a** with increasing temperature. As the Cu···Cu distance is increased (large arrows), the I···I distance decreases (large arrows), the Cu–I–Cu angles increase (curved arrows), and the I–Cu–I angles decrease (curved arrows).

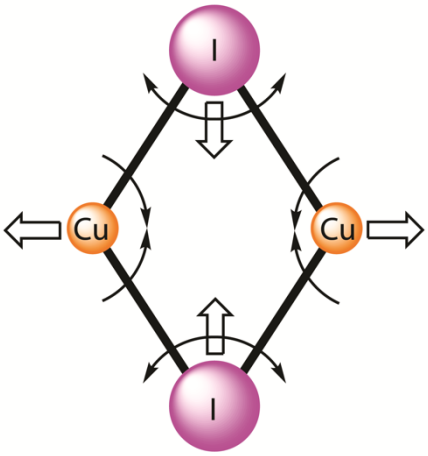

An X-ray structural determination of $Cu_4I_4Py_4$ (**2**) was carried out at 100 K, see Figure 10. In this case the new structural analysis was consistent with the previously reported ambient temperature determination [1]. As is apparent from data in Table 2, Cu···Cu distances in **2** are seen to contract on average by 0.020 Å between 295 and 100 K. However, the I···I distances remain nearly constant upon cooling, decreasing by only 0.005 Å on average. Once again, this is likely the result of bond lengthening being offset by ring flexure.

Figure 10. Thermal ellipsoid (50%) drawing of **2** at 100 K.

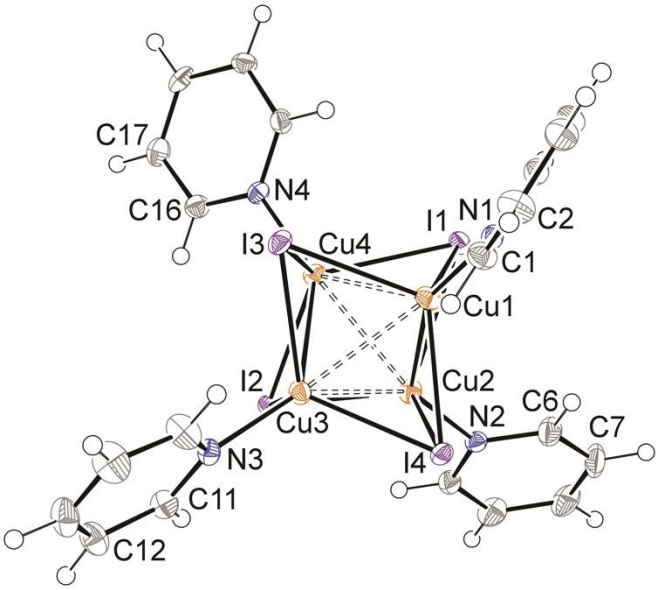

Based on the foregoing results, we are able to correlate the luminescence data to the X-ray structural data as a function of temperature. This is the first report that combines luminescence and X-ray structural data for the dimer as a function of temperature, allowing more detailed photophysical analysis of **1a**. Upon cooling from 250 to 100 K, the X-ray structural data reveal no change in the crystalline phase for **1a**. As described above, we see contraction of the Cu–I–Cu angle and expansion of the I–Cu–I angle, which results in shorter Cu···Cu distances at lower temperatures. This variation in Cu···Cu distance has been discussed as an important factor in determining the luminescence properties of Cu_nI_n cluster crystals [20]–[23]. This dependence becomes clear when comparing the Cu···Cu distance and low energy maximum emission peak wavelength over varying temperatures as seen in Figure 11. The linear change in Cu···Cu distance directly correlates with a linear shift of the emission energy and further supports the CC assignment of this peak.

Figure 11: Comparison of the (left) Cu···Cu distance, (middle) CC emission peak wavelength, and (right) XLCT intensity with varying temperature.

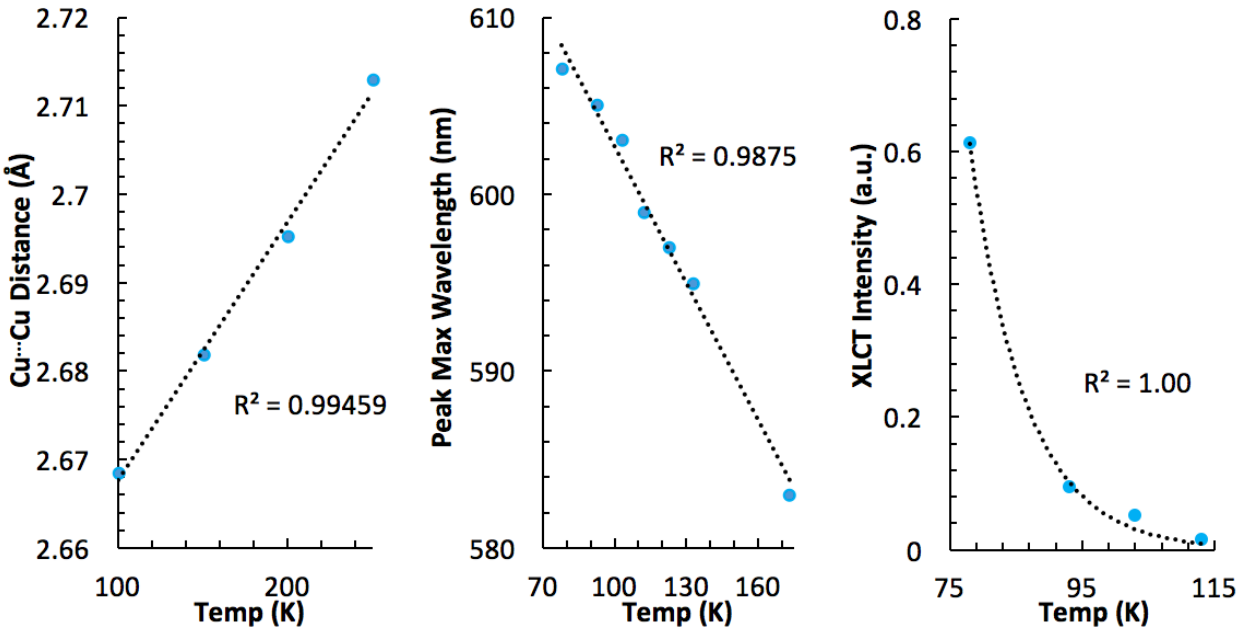

Conclusions:

We have reported a new polymorph of the 1:2 CuI:pyridine complex, **1a**. The structure of **1a** has been assigned as an iodine-bridged dimer, $Cu_2I_2Py_4$, rather than a chain, $(CuIPy_2)_n$. This assignment was based on spectroscopic evidence for Cu_nI_n cluster behavior and the prevalence of Cu_2I_2 dimers in the literature. Excitation at high energies reveal a complex emission spectrum containing XLCT, XMLCT, and CC transitions. In conjunction with the DRS spectra, a DFT and TD-DFT analysis suggest this is the result of excitation of a CC absorption band. Comparison of **1a** to known dimer polymorph **1b** reveals a longer, albeit still formally bonding, Cu···Cu distance for the new polymorph. A combination of variable temperature crystallography and luminescence spectroscopy has clearly demonstrated the Cu···Cu distance dependence of emission energies for **1a**. Results demonstrate that the luminescence bands in $Cu_2I_2Py_4$ can be tuned as a function of temperature. A low-temperature X-ray structure of the cubane tetramer $Cu_4I_4Py_4$, **2**, has also been reported and shows contraction of the Cu_4I_4 cluster.

Supplementary Material: Crystallographic information on CCDC 1529200-1529204 can be obtained free of charge by e-mailing data_request@ccdc.cam.ac.uk or by contacting The Cambridge Crystallographic Data Centre, 12 Union Road, Cambridge, CB2 1EZ UK; Fax +44(0)1223-336033; www.ccdc.cam.ac.uk/data_request/cif.

Acknowledgement. We are indebted to NSF (CHE-0443345) and the College of William and Mary for the purchase of the X-ray equipment.

References:

(1) C.L. Raston, A.H. White, J. Chem. Soc., Dalton Trans. 2153 (1976).
(2) A. Bondi, J. Phys. Chem. 68, 441 (1964).
(3) (a) K.R. Kyle, C.K. Ryu, J.A. DiBenedetto, P.C. Ford, J. Am. Chem. Soc. 113, 2954 (1991). (b) P.C. Ford, E. Cariati, J. Bourassa, Chem. Rev. 99, 3625 (1999). (c) M. Vitale, P.C. Ford, Coord. Chem. Rev. 219–221, 3 (2001).
(4) E. Eitel, D. Oelkrug, W. Hiller, J. Strähle, Z. Naturforsch. 35b, 1247 (1980).
(5) J.C. Dyason, L.M. Engelhardt, P.C. Healy, A.H. White, Aust. J. Chem. 37, 2201 (1984).
(6) P.M. Graham, R.D. Pike, M. Sabat, R.D. Baily, W.T. Pennington, Inorg. Chem. 39, 5121 (2000).
(7) *SAINT PLUS*: Bruker Analytical X-ray Systems: Madison, WI, 2001.
(8) *SADABS*: Bruker Analytical X-ray Systems: Madison, WI, 2001.
(9) G.M. Sheldrick, Acta Crystallogr., Sect. A 64, 112 (2008).
(10) C.B. Hübschle, G.M. Sheldrick, B. Dittrich, J. Appl. Cryst. 44, 1281 (2011).
(11) *Diffrac-EVA 3.1*: Bruker Analytical X-ray Systems: Madison, WI, 2012.
(12) *Mercury 3.9*: Cambridge Crystallographic Data Centre (2016).
(13) M.J. Frisch, G.W. Trucks, H.B. Schlegel, G.E. Scuseria, M.A. Robb, J.R. Cheeseman, G. Scalmani, V. Barone, B. Mennucci, G.A. Petersson, H. Nakatsuji, M. Caricato, X. Li, H.P. Hratchian, A.F. Izmaylov, J. Bloino, G. Zheng, J.L. Sonnenberg, M. Hada, M. Ehara, K. Toyota, R. Fukuda, J. Hasegawa, M. Ishida, T. Nakajima, Y. Honda, O. Kitao, H. Nakai, T. Vreven, J.A. Montgomery, Jr., J.E. Peralta, F. Ogliaro, M. Bearpark, J.J. Heyd, E. Brothers, K.N. Kudin, V.N. Staroverov, T. Keith, R. Kobayashi, J. Normand, K. Raghavachari, A. Rendell, J.C. Burant, S.S. Iyengar, J. Tomasi, M. Cossi, N. Rega, J.M. Millam, M. Klene, J.E. Knox, J.B. Cross, V. Bakken, C. Adamo, J. Jaramillo, R. Gomperts, R.E. Stratmann, O. Yazyev, A.J. Austin, R. Cammi, C. Pomelli, J.W. Ochterski, R.L. Martin, K. Morokuma, V.G. Zakrzewski, G.A. Voth, P. Salvador, J.J. Dannenberg, S. Dapprich, A.D. Daniels, O. Farkas, J.B. Foresman, J.V. Ortiz, J. Cioslowski, and D.J. Fox, Gaussian, Inc., Wallingford CT, 2010.
(14) A.D. Becke, J. Chem. Phys. 98, 5648 (1993).
(15) C. Lee, W. Yang, R.G. Parr, Phys. Rev. B 37785 (1988).
(16) Cambridge Crystallographic Database accessed 1-6-17.

(17) See e.g. (a) P.C. Healy, C. Pakawatchai, A.H. White, J. Chem. Soc., Dalton Trans. 1917 (1983). (b) W. Hiller, Z. Naturforsch., B: Chem. Sci. 39, 861 (1984). (c) P.C. Healy, C. Pakawatchai, A.H. White, J. Chem. Soc., Dalton Trans. 2531 (1985). (d) N.P. Rath, E.M. Holt, K. Tanimura J. Chem. Soc., Dalton Trans. 2303 (1986). (e) A.J. Blake, N.R. Brooks, N.R. Champness, P.A. Cooke, M. Crew, A.M. Deveson, L.R. Hanton, P. Hubberstey, D. Fenske, M. Schroder Cryst. Eng. 2, 181 (1999). (f) S.R. Batten, J.C. Jeffery, M.D. Ward, Inorg. Chim. Acta 292, 231 (1999). (g) D.A. McMorran, P.J. Steel, J. Chem. Soc., Dalton Trans. 3321 (2002). (h) C. Nather, I. Jess, N. Lehnert, D. Hinz-Hubner, Solid State Sci. 5, 1343 (2003). (i) C.M. Fitchett, P.J. Steel, Polyhedron 27, 1527 (2008). (j) E. Haldon, E. Alvarez, M. C. Nicasio, P. J. Perez, Organometallics 28, 3815 (2009). (k) W. Liu, Y. Fang, G. Z. Wei, S. J. Teat, K. Xiong, Z. Hu, W. P. Lustig, J. Li, J. Am. Chem. Soc. 137, 9400 (2015).

(18) (a) H. Kitagawa, H. Ohtsu, M. Kawano, Angew. Chem. Int. Ed. 52, 12395 (2013). (b) H. Kitagawa, H. Ohtsu, A.J. Cruz-Cabeza, M. Kawano, IUCrJ 3, 232 (2016).

(19) (a) X. Haiyan, I. Kinoshita, T. Karasawa, K. Kimura, T. Nishioka, I. Akai, K. Kanemoto, J. Phys. Chem. B 109, 9339 (2005). (b) I. Krytchankou, I. Koshevoy, V. Gurzhiy, V. Pomogaev, S. Tunik, Inorg. Chem. 54, 8288 (2015). (c) H. Rasika Dias, H. Diyabalanage, M. Rawashdeh-Omary, M. Franzman, M. Omary, J. Am. Chem. Soc. 125, 12071 (2003).

(20) F. DeAngelis, S. Fantacci, A. Sgamellotti, E. Cariati, R. Ugo, P. Ford, Inorg. Chem. 45, 10576 (2006).

(21) K. Shimada, A. Kobayashi, Y. Ono, H. Ohara, T. Hasegawa, T. Taketsugu, E. Sakuda, S. Akagi, N. Kitamura, M. Kato, J. Phys. Chem. C 120, 16002 (2016).

(22) A. Tsuboyama, K. Kuge, M. Furugori, S. Okada, M. Hoshino, K. Ueno, Inorg. Chem. 46, 1992 (2007).

(23) Y. Okano, H. Ohara, A. Kobayashi, M. Yoshida, M. Kato, Inorg. Chem. 55, 5227 (2016).

(24) Ford. P. Cariati, E. Bourassa, J. Chem. Rev. 99, 3625 (1999).

(25) De Angelis, F. Fantacci, S. Sgamelloti, A. Cariati, E. Ugo, R. Ford, P. Inorg. Chem. 45, 10576 (2006).

Table 1. Crystal and Structure Refinement Data.

	$Cu_2I_2Py_4$, **1a**	$Cu_2I_2Py_4$, **1b** [4]	$Cu_4I_4Py_4$, **2** (100 K)	$Cu_4I_4Py_4$, **2** (295 K) [2]
CCDC deposit	1529200	DEJYOG	1529204	CUIPYR
color and habit	Colorless plate	Colorless block	Colorless block	Colorless block
size, mm	0.43 × 0.17 × 0.05	0.25 × 0.25 × 0.25	0.24 × 0.22 × 0.22	0.12 × 0.12 × 0.12
formula	$C_{20}H_{20}Cu_2I_2N_4$	$C_{20}H_{20}Cu_2I_2N_4$	$C_{20}H_{20}Cu_4I_4N_4$	$C_{20}H_{20}Cu_4I_4N_4$
formula weight	697.28	697.28	1078.16	1078.16
space group	$P4_12_12$	$C222_1$	$P2_12_12_1$	$P2_12_12_1$
a, Å	8.4369(10)	14.578(4)	11.7174(5)	16.032(6)
b, Å	8.4369(10)	10.448(3)	15.2738(7)	15.510(2)
c, Å	32.195(4)	31.559(7)	15.7404(7)	11.756(3)
volume, $Å^3$	2291.7(6)	4807(2)	2817.0(2)	2923(2)
Z	4	8	4	4
ρ_{calc}, g cm^{-3}	2.021	1.93	2.542	2.44
F_{000}	1328	2656	1984	1984
μ(Mo Kα), mm^{-1}	4.563	4.5	7.378	7.28
radiation	MoKα (λ = 0.71073 Å)	MoKα (λ = 0.71073 Å)	MoKα (λ = 0.71073 Å)	MoKα (λ = 0.71073 Å)
temperature, K	100	295	100	295
residuals:[a] R; R_w	0.0125, 0.0301	N.R.	0.0107, 0.0272	N.R.
goodness of fit	1.131	N.R.	0.959	N.R.
Flack	0.20(3)	N.R.	N.R.	0.027(15)

[a] $R = R_1 = \Sigma||F_o| - |F_c||/\Sigma|F_o|$ for observed data only. $R_w = wR_2 = \{\Sigma[w(F_o^2 - F_c^2)^2]/\Sigma[w(F_o^2)^2]\}^{1/2}$ for all data.

Table 2. Selected bond lengths (Å) and angles (°).

	$Cu_2I_2Py_4$, **1a** (100 K)	$Cu_2I_2Py_4$, **1b** (295 K) [4]	$Cu_4I_4Py_4$, **2** (100 K)	$Cu_4I_4Py_4$, **2**, (295) K [2]
Cu···Cu	2.6686(9)	2.669(5)	2.5922(6)– 2.7050(6)	2.619(5)–2.722(5)
Cu–I	2.611(3), 2.618(3), 2.626(4), 2.653(4)	2.628(4), 2.629(4), 2.642(4), 2.656(4)	2.6242(5)–2.7909(5)	2.629(4)–2.790(4)
Cu–N	1.948(19), 2.02(2), 2.073(3), 2.075(3)	2.02(2), 2.06(2), 2.07(3), 2.08(3)	2.020(3), 2.030(3), 2.031(3), 2.040(3)	2.02(2), 2.04(2), 2.05(2), 2.06(2)
I···I	4.525(5)	4.536(3)	4.4300(3)–4.6005(3)	4.442(3)–4.594(3)
I–Cu–I	118.31(18), 119.58(18)	117.8(1), 119.2(1)	110.473(16)– 120.779(18)	110.4(1)–120.2(1)
N–Cu–N	103.7(9), 103.8(9)	100.9(12), 102.3(11)	–	–
I–Cu–N	102.59(17)–114.5(8)	106.6(10)–111.4(7)	95.05(8)– 112.12(8)	95.2(6)–111.4(6)
Cu–I–Cu	60.92(7), 61.18(8)	61.4(1), 61.6(1)	57.101(13)– 60.922(14)	57.7(1)–61.1(1)

Table 3. Variable temperature data for selected bonds lengths (Å) and angles (°) in **1a**.

	100 K	150 K	200 K	250 K
Cu1a···Cu1b	2.6686(9)	2.6819(10)	2.6952(10)	2.7129(12)
Cu1a–I1a	2.611(3)	2.619(3)	2.620(3)	2.622(3)
Cu1a–I1b	2.626(4)	2.629(5)	2.629(4)	2.632(5)
Cu1b–I1a	2.653(4)	2.656(4)	2.657(4)	2.661(4)
Cu1b–I1b	2.618(3)	2.625(3)	2.623(3)	2.630(3)
Cu1a–N1a	2.02(2)	2.00(2)	2.00(2)	2.01(2)
Cu1a–N2a	2.073(3)	2.076(3)	2.076(3)	2.074(4)
Cu1b–N1b	1.948(19)	2.00(2)	2.00(2)	2.00(2)
Cu1b–N2b	2.075(3)	2.076(3)	2.078(3)	2.081(4)
I1a···I1b	4.525(5)	4.530(5)	4.523(4)	4.479(5)
Cu1a–I1a–Cu1b	60.92(7)	61.11(8)	61.42(7)	61.80(7)
Cu1a–I1b–Cu1b	61.18(8)	61.39(9)	61.74(8)	62.07(8)
I1a–Cu1a–I1b	119.58(18)	119.33(19)	118.98(17)	118.73(18)
I1a–Cu1b–I1b	118.31(18)	118.16(19)	117.85(18)	117.39(19)

Table 4. Tabulated DFT ground state geometrical parameters for **1a**.

	Calculated Bond Length (Å), Angle (°)		
	Monomer	Dimer	Experimental
Cu···Cu	2.880	3.322	2.6686
Cu–I	2.839	2.93	2.627*
Cu–N	2.059	2.06	2.029*
I···I	4.892	4.714	4.525
I–Cu–I	119.0	107.03	118.95*
N–Cu–N	122.1	121.7	103.8*
I–Cu–N	105.2	107.09	108.5*
Cu–I–Cu	61.0	69.3	61.1*

*Indicates averaged values